Materials & Design 245 (2024) 113243

Contents lists available at ScienceDirect

Materials & Design

journal homepage: www.elsevier.com/locate/matdes

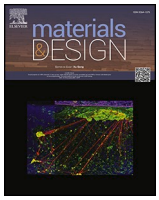

Effect of laser drilling on biomorphically engineered hydroxyapatite scaffolds derived from rattan wood

Evangelos Daskalakis [a,b,*], Neelam Iqbal [a,b], Sarathkumar Loganathan [a], Emilio Spettoli [e], Giacomo Morozzi [e], Alberto Ballardini [e], Peter V. Giannoudis [c,d], Animesh Jha [a,d]

[a] School of Chemical and Process Engineering, University of Leeds, Leeds LS2 9JT, UK
[b] Oral Biology Division, School of Dentistry, University of Leeds, Leeds LS2 9JT, UK
[c] Academic Department of Trauma and Orthopaedic Surgery, School of Medicine, University of Leeds, Leeds LS2 9JT, UK
[d] NIHR Leeds Biomedical Research Centre, Chapel Allerton Hospital, Leeds LS2 9LU, UK
[e] GreenBone Ortho SpA, Via Albert Einstein, 848018 Faenza RA, Italy

ARTICLE INFO

Keywords:
Laser drilling
Biomorphic Scaffolds
Bone defect restoration
Osteoconduction
Compressive strength

ABSTRACT

The restoration of critical-size load-bearing bone defects calls for the application of bioactive scaffolds that are regenerative, osteoconductive, and demonstrate mechanical strength comparable with natural bone. Novel hydroxyapatite (HAp) scaffolds sourced and fabricated through the biomorphic transformation of rattan wood (GreenBone-GB) were laser-drilled (LD) with parallel and lateral sub-millimetre channels, which enhanced the overall porosity for promoting the flow of cells and fluids throughout the scaffolds. The compositional analysis of the LD scaffolds confirmed the presence of the $Ca_5(PO_4)_3OH$ and $Ca_3(PO_4)_2$ phases, with no evidence of drilling contamination. Water jet laser drilling enhanced the interconnecting porosity of the morphogenic scaffolds by 22.5 %, without obstructing the intrinsic uniaxial fibrous structure inherited from rattan wood. Across eight varied drilled patterns, the resulting scaffolds preserved the structural integrity and exhibited compressive strength ranging from 6.74 ± 1.25 to 10.18 ± 0.43 MPa, while the Vickers Hardness was comparable with natural bone. Cell viability assessments confirmed that the LD scaffolds exhibited no toxicity and presented >90 % cell viability. We demonstrate that laser drilling effectively enhanced the pore volume for improved osteoconductivity via cell migration in the bio-morphogenic GB-structure. Since the GB scaffolds are CE-marked products, laser drilling for pore surface engineering could provide improved scaffolds for clinical use.

1. Introduction

Compromised bone healing, resulting from fractures or defects, can lead to delayed/missed union and non-union of bone, necessitating revision surgeries, which places a heavy burden on the patients' health and strains the healthcare system [1,2]. The lack of vascularisation due to disruption in angiogenesis may induce infection at the healing site, leading to tissue necrosis [3]. One of the key challenges in orthopaedic surgery is repairing critical-size load-bearing bone defects. The diamond concept [6] explains that the use of regenerative scaffolds infused with the patient's own bone marrow pluripotent mesenchymal stromal cells (BMMSCs) to initiate osteoinductive, conductive, and angiogenic processes to compensate for substantial bone loss [2,4–7]. Additionally, synthetic bone scaffolds should foster cell attachment and provide three-dimensional features that facilitate the easy handling and fitting of the graft into the defect area [4,8]. The co-occurrence of osteogenesis and angiogenesis from BMMScs present within a scaffold is essential for sustaining resorption, remineralisation and new bone formation. It is essential for this reason a bone scaffold must exhibit interconnective porosity to maintain a complex hierarchy of molecular communication during the bone formation leading to healing, allowing for the cross-flow of cellular micronutrients and the removal of cellular waste via the vascular network [7].

In clinical scenarios, various graft and scaffold options include autografts, allografts, xenografts, calcium phosphate cement, and combinations of bio-ceramic grafts [9]. Autografts are preferred over allografts due to their superior regenerative capabilities. However, autografts require an additional surgical site which often leads to surgical morbidity, while the graft quantity is limited [10]. Xenografts are rarely used due to their higher risk of implant rejection or infection [9,10]. For

* Corresponding author.
E-mail address: E.Daskalakis@leeds.ac.uk (E. Daskalakis).

https://doi.org/10.1016/j.matdes.2024.113243
Received 10 May 2024; Received in revised form 19 July 2024; Accepted 10 August 2024
Available online 5 September 2024

bio-ceramic bone graft substitutes, it is crucial to optimise the physical pore structure and chemistry [8] due to the direct correlation between macro porosity, pore size, porosity volume, interconnection size, and density of bio-ceramics graft substitutes to the rate and quality of their integration with bone. Optimising the pore structure of biomaterials can influence cellular interactions involving adhesion, proliferation, and migration, enhancing tissue regeneration [11,12]. Efficient nutrient and waste exchange through pores is essential for cell viability and function, promoting healthy tissue development [13]. Both resorbable and non-resorbable bio-ceramics influence the bioactivity in bone through direct mechanisms involving dissolution and release of ionic products *in vivo* and indirectly through surface protein adsorption and cell behaviour [14]. From the list of different types of bioceramics, the hydroxyapatite ($Ca_{10}(PO_4)_6(OH)_2$) and α,β-tricalcium phosphates (β-$Ca_3(PO_4)_2$, α-$Ca_3(PO_4)_2$) are bioactive and resemble natural bone apatite, but these minerals display poor tensile strength and brittleness. The commercially available bioactive glasses ($CaO–SiO_2–P_2O_5$) are osteoinductive and non-cytotoxic, but they are fragile and demonstrate low toughness. Zirconia (ZrO_2) and aluminium oxide (Al_2O_3) are known for their corrosion resistance biological and chemical inertness, however these two ceramic oxides are bio-inert and lack bioactivity [15]. Commercially available bio-ceramic bone graft substitutes demonstrate micropores in the range of 1–2 μm, macropores of 100 – 1000 μm and volumetric porosity between 50 to 70 % [14,16]. Hydroxyapatite based biomaterials reported in the literature are summarised in Supplementary S1.1.

The GreenBone (GB) scaffold is a novel bio-ceramic CE-marked medical device manufactured through the 6-step biomorphic transformation of rattan wood [17,18]. Similarly to the morphogenic structure of rattan wood, the scaffold is characterised by long axial channels with variable lumen diameters (from 10 to 500 μm, ~300 μm), which are well-suited for blood vessel ingrowth. The inherited asymmetric axial pores, approximately 60 vol%, resemble the structure of the osteogenic system, and aid with bone regeneration due to allowing cell migration and proliferation across the whole length of the scaffold [17,18]. The low-temperature processing employed throughout the manufacturing process does not involve sintering and facilitates the preservation of a crystalline sub-micron hydroxyapatite structure, which enhances the bioactivity of the GB scaffolds compared to conventional synthetic sintered bio-ceramics [17,18]. The hydroxyapatite matrix of the GB scaffolds is doped with Mg^{2+} and Sr^{2+} ions during fabrication, which is known to augment biocompatibility, promote osteogenesis, and improve mechanical properties [17,18]. Tampieri et al. [17] demonstrated the superiority of the biomorphic GB scaffolds in addressing clinical needs by harnessing the biomimetic concept to favour tissue regeneration when compared to commercial sintered hydroxyapatite scaffolds from Engipore™; Fin-Ceramica Faenza, Italy (HA~5 wt% of β-TCP, macro pore size 100–200 μm and porosity ~60 vol%.) [19]. Additionally, the mechanical properties of the material allow easy customisation, in the operating room, for fitting in the bone defects. The scaffolds maintain structural integrity even after breakage, absorbing microtraumas, which makes them suitable for load-bearing applications [17,19]. Sprio et al. [18] compared the compressive strength of the biomorphic GB scaffolds (9.8 ± 5.9 MPa) to commercial sintered scaffolds from Kasios®, Atoll (HA-β-TCP ~25 %, porosity 64 ± 4 vol%), 5.7 ± 1.6 MPa.

The bio-morphogenic structure of the GB scaffolds allows cellular and fluid transport primarily in the axial direction, which limits the osteoconductivity of the graft after surgery [2]. For that reason we employed laser drilling to increase the pore volume by drilling axial and transverse channels in the GB scaffolds. Laser drilling enables high precision “cold” processing, flexibility in drilling geometry and wear-free machining due to the contactless nature of lasers [20]. Laser drilling is preferred over mechanical drilling particularly for fragile bio-ceramics, as it prevents the i) induction of fractures, ii) generation of dust and debris, and iii) introduction of contamination [21]. Several studies demonstrate laser drilling of biomaterials performed by pulsed femtosecond lasers [22–24]. Among the beam controlling mechanisms utilised, spiral laser trepanning involves the laser beam gradually removing material from the edges of the holes, in a spiral pattern, forming well-defined geometries [20,25]. In comparison, laser milling achieves drilling by scanning the entire volume of the hole and ablating material across the beam path [26]. Previous literature has primarily concentrated on laser machining of natural bone, as well as laser processing in dental restoration applications, which involves reshaping, bone repair, tooth restoration and scaffold fixing [7,23,27,28].

We aim to develop a non-intrusive laser drilling methodology for promoting the osteoconductive and cell migrating potential of the biomorphic GB scaffolds, without compromising the regulatory approved CE-marked medical device. Our objectives are to enhance the pore volume of the scaffolds for advanced cellular transport without i) compromising the structural integrity, ii) obstructing the natural porosity or iii) inducing toxicity in the scaffolds. The desired pore size distribution should fall within the range of 200 to 1000 μm, ensuring that the microscopic channels adequately supply nutrients throughout the scaffold. With in-theatre laser surgery becoming popular, engineering evidence on laser drilling as an exogenous intervention suggests it could enhance the osteoconductivity of various scaffolds, implants, and fixators.

2. Materials and methods

The reference GB scaffolds (D = 10 mm and H=4 mm) possess long axial channels of varying diameters, inherited from rattan wood, Fig. 3-A. The chemical composition of the GB scaffolds has been previously reported as $Ca_5(PO_4)_3OH$ (hydroxyapatite) and $Ca_3(PO_4)_2$ (β-tricalcium phosphate) at a (85:15) ratio [17,18]. The samples have been supplied by the GreenBone Ortho Company (Italy).

2.1. Drilling methods

Three drilling techniques were employed for enhancing the interconnected porosity of the scaffolds:

i) Fig. 1-A demonstrates water jet laser drilling of the GB scaffolds, performed in a helical pattern by a SYNOVA MCS300 (Nd:YAG pulsed water jet laser). Following parameter optimisation the operating laser output power was set to 31 W for the operating wavelength of 532 nm (green laser). The working frequency was set to 6 kHz and the pulse width was 250 ns at FWHM. The diameter of the water jet was 50 μm, which was coming out of the nozzle at the pressure of 300 bar.
ii) Fig. 1-B demonstrates femtosecond laser drilling performed by a Ti Sapphire femtosecond laser (COHERENT Libra) operating at 800 nm wavelength, 1 kHz repetition rate, 100 fs pulse duration and 5 mJ pulse energy. A 6.2 mm focal lens was used, and the working stage was controlled by CNC-controlled XYZ-Stage with a resolution of 100 nm.
iii) For comparison purposes, Fig. 1-D demonstrates conventional drilling by a drill bit of D=0.7 mm at 200 rpm.

Water jet laser drilling was performed in a helical pattern and it involved the laser beam gradually removing material from the circumference of each sub-mm through-hole in a spiral pattern. The process of drilling 9 through axial holes (D=0.7 mm) on the GB scaffolds, for the operating parameters forementioned, required approximately 1 min. The code and beam path followed for performing water jet laser drilling are available in the Supplementary S2.1.

During femtosecond laser drilling, four different pulse overlapping parameters were tested by controlling the working stage through 4 different codes. The average power and scanning velocity were set to 0.5 mJ and 1 mm/s respectively for enabling drilling through multiple

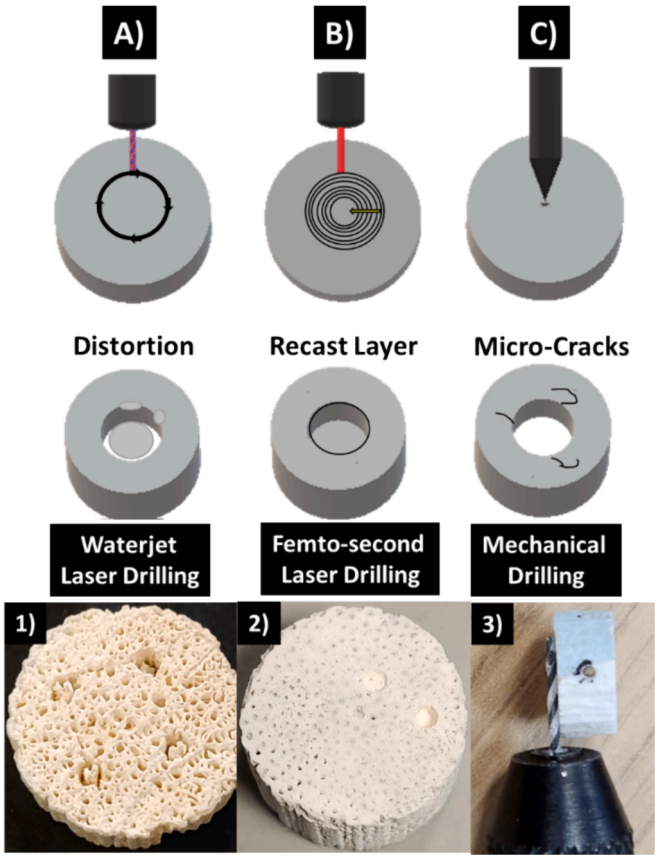

Fig. 1. GreenBone (GB) scaffolds were processed via four drilling techniques: A) Water jet laser drilling. B) Femtosecond laser drilling C) Mechanical drilling.

overlapping scanning layers. The pulse overlapping provided by Codes 1, 2 and 3 were 0.05, 0.005 and 0.0025 mm respectively. The effect of each overlapping parameter on the GB scaffolds is demonstrated in Fig. 2. The codes corresponding to each drilling parameter and pattern are included in the Supplementary S2.2. The pulse overlapping provided by code 1 was not adequate for laser milling the scaffolds. Code 3 demonstrated the finest pulse overlapping, however code 2 displayed sufficient pulse overlapping for achieving laser milling in a shorter duration. The maximum depth of the drilled hole when using the femtosecond laser was approximately 2 mm due to restrictions related to the focal lens. Laser milling with code 2 required approximately 10 min for drilling a 2 mm hole, due to the low repetition rate used.

Conventional mechanical drilling effectively formed through holes, but it did not provide consistent results, due to: i) the formation of microcrakcs, and ii) crumbling of samples during drilling. The rate of material removal for each of the drilling techniques are summarised in Table 1. Overall, water jet laser drilling was selected as the most suitable drilling mechanism for enhancing the pore volume of the LD GB scaffolds, due to its high speed, efficiency and precision.

Table 1
The material removal rate for each drilling method on the Green Bone scaffolds.

Drilling Technique	Material Removal Rate (mm^3/s)
Water Jet Laser	0.1–0.23
Femtosecond Laser	0.008
Conventional Drilling	0.025–0.033

2.2. Drilling plan

The next step of the machining process involved optimising the arrangement of the drilled-holes, on the GB scaffolds, for enhancing the interconnected porosity. The reference GB scaffolds were laser-drilled parallelly and perpendicularly to the natural axial porosity of the scaffolds. The diameter of the laser-drilled channels ranged between 200 and 1000 μm to enable sufficient nutrient supply for cellular growth. Fig. 3-B demonstrates the four parallelly drilled GB scaffolds exhibiting 4, 5, 6 and 9 holes, where the holes were produced in a dice-like configuration. Fig. 3-C displays the perpendicularly drilled GB scaffolds consisting of 2, 3 and 4 through-holes. The drilled channels intersected at the centre of the cylindrical scaffolds, at angles of 90°, 60° and 45° for the 2-hole, 3-hole and 4-hole samples respectively.

2.3. Drilled GreenBone scaffolds

Fig. 4 exhibits the reference unmodified and the water jet LD GB scaffolds deriving from the drilling plan of Fig. 3. Figs. 4-1D demonstrates a GB scaffold which combines 9 parallel and 4 perpendicular holes, which are the maximum number of permissible holes on the reference GB scaffolds without compromising the structural integrity. To preserve the structural integrity of the GB scaffolds during processing and to ensure consistent results, the samples undergoing laser drilling must display stringent size tolerance, which is required during the clamping process. A stainless-steel holder, equipped with a protective cover, protected the scaffolds from any potential damage during drilling, Fig. 4-2.

2.4. Characterisation methods

The phase identification in the pre-and post-drilled GB scaffolds was made through X-Ray diffraction (XRD) using a Bruker D8 Advance (monochromatic CuK_α radiation of ($\lambda = 0.15417$ nm), 2θ range 10–80°). SEM and EDS analysis was performed by a Hitachi SU8230. A ThermoFisher Scientific He-Pycnometer measured the skeletal density of the scaffolds. The profile of the unmodified and LD GB scaffolds was observed with the assistance of an InfiniteFocus Alicona profilometer and a Carl Zeiss LSM800 Mat CLSM confocal microscope, while the raw data of the surface roughness was processed with a Gaussian filter for inclined planar surfaces (ISO 16610–61, Default Linear Planar, Order 1). A more detailed description of the experimental parameters is available

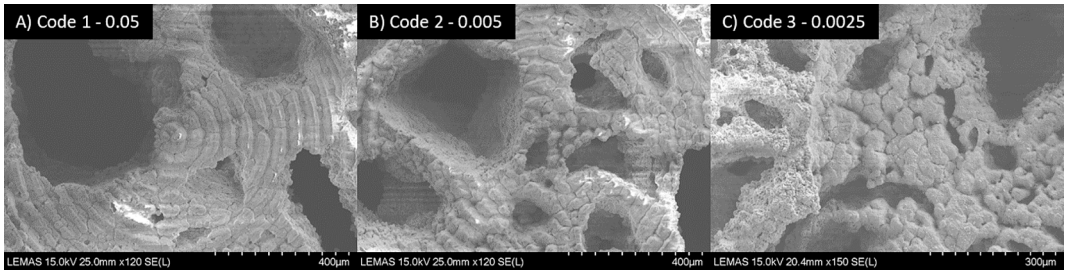

Fig. 2. The pulse overlapping when performing laser drilling with the Ti sapphire fs laser on the GB scaffolds provided by: A) Code 1: 0.05 mm, B) Code 2: 0.005 mm and C) Code 3: 0.0025 mm.

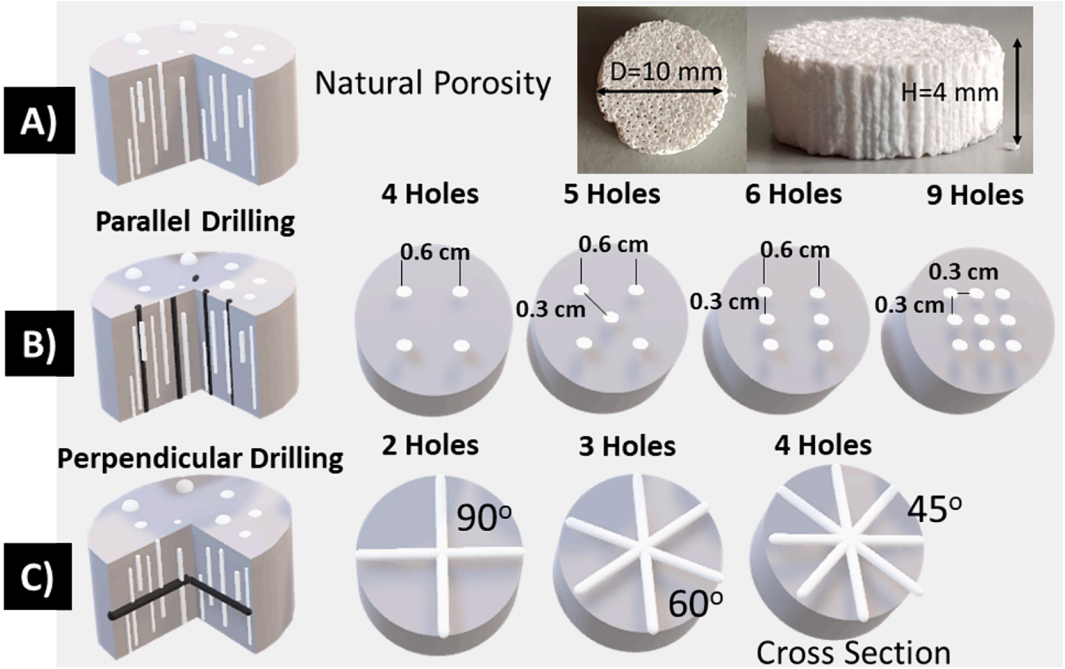

Fig. 3. The laser drilling plan. A) The orientation of the natural porosity of the GreenBone (GB) scaffolds, based on which parallel and perpendicular drilling were performed. B) Parallel drilling of 4, 5, 6 and 9 holes. C) Perpendicular drilling of 2, 3 and 4 through holes.

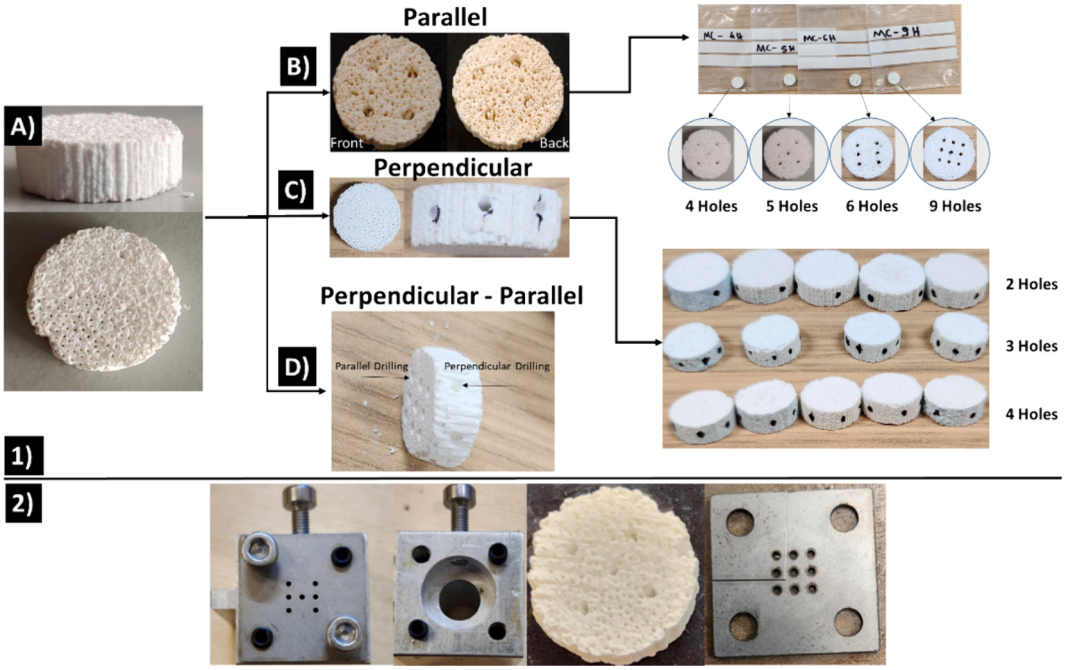

Fig. 4. 1-A) The reference GB Scaffold. 1-B) Parallelly LD GB scaffolds with 4, 5, 6 and 9 holes. 1-C) Perpendicularly LD GB scaffolds with 2, 3 and 4 holes. 1-D) Sample laser drilled with 4 perpendicular and 9 parallel holes. 2) Protective cover for preventing the samples from getting damaged during water jet laser drilling.

at the Supplementary S2.3.

2.5. Mechanical testing equipment

The compressive strength (Instron equipment) of the scaffolds (n = 12) was tested according to the ISO standard 13175–3. The Vickers microhardness (BUEHLER Wilson Hardness) of the GB scaffolds was measured for the available loads of 1, 2, 3 and 5 kg.

2.6. In vitro testing

The 4-hole perpendicularly LD GB scaffolds (10 mm diameter, 4 mm height) were selected for *in-vitro* analysis due to accommodating the highest number of permissible transverse holes for improved interconnected porosity, without significantly compromising the compressive strength of the scaffolds. The cell viability assessments were carried out using G292 osteoblast cells. The LD scaffolds were examined for contact cytotoxicity (48 h to 7 days) according to ISO10993-5:2002(E)

Part 5, and were categorised based on their reactivity grade. The indirect cytotoxicity of GB scaffolds was assessed using the XTT assay at time points of 72 h, 1, 2, 3 and 4 weeks, according to ISO 10993:2021 Part 12, and ISO 10993–5:2009(E) Part 5. The G292 cell viability assessment was performed by Live/Dead assay, 72 h after the LD scaffolds were seeded and incubated. The G292 cell attachment and proliferation on the GB scaffolds were verified by Fluorescence Actin and Nuclei Staining (Alexa Fluor and DAPI), performed on LD GB samples 72 h after seeding. A detailed description of the experimental procedure for all in vitro analysis techniques can be found in the supplementary information Supplementary S2.4.

2.7. Degradation testing

The structural and physiological integrity of the unmodified and LD GB scaffolds was evaluated after submerging the scaffolds (N=3) in phosphate-buffered saline solution. The time points selected were 2 days, 5 days and 10 days. The wet scaffolds were furnace dried at 50 °C for 24 h before measuring the weight. The percentage of weight loss was calculated using Equation (1), where W_0 = Initial scaffold weights W_{d1} = Scaffold weights, t = Time.

$$\Delta W0(\%) = \left[\frac{W0 - Wd1}{W0}\right] \times 100 \quad (1)$$

The extracted solutions at each time point were analysed using a Renishaw inVia Raman microscope with a laser excitation source at a 785 nm wavelength. The aim was to identify if minerals were released in the solution by the unmodified and LD GB scaffolds. A more detailed description of the procedure is included in Supplementary S2.3.

2.8. Statistical analysis

The information is displayed as averages along with their respective ± standard deviations. A two-way ANOVA was employed to assess variations among groups. Statistical computations and visual data representations were conducted using GraphPad Prism (version 9.2.0, USA), and significance was determined at a p-value of < 0.05.

3. Results

3.1. X-ray diffraction

Fig. 5 demonstrates the XRD plots of the unmodified and water jet laser-drilled GB scaffolds. No damage or laser processing related contamination occurred during the drilling process, as the XRD plot of the laser-drilled scaffold is comparable to the diffractogram of the reference sample. The analysis demonstrated that all samples consisted of two main phases, $Ca_5(PO_4)_3OH$ and $Ca_3(PO_4)_2$, commonly known as hydroxyapatite and β-tricalcium phosphate, indicating that laser drilling did not alter the composition of the GB scaffolds. The Sr-CP and Mg-CP phases detected in the scaffolds were a result of a doping step in the manufacturing process [17]. Tampieri et al. [17] demonstrated that the multiple ion substitution slightly shifted the peak position in the diffractograms of the GB scaffolds when compared to stoichiometric hydroxyapatite and beta-tricalcium phosphate phases.

3.2. Volumetric porosity and pore volume increase

The geometrical density of the GB scaffolds was compared to the density measured by Helium (He) Pycnometry to identify the volumetric porosity of the scaffolds. The mass of the reference GB scaffold (D=10 mm and H=4 mm) is 0.42 g, its volume when excluding porosity is 314 mm^3 and its geometrical density is 1.33 g/cc. The surface area of the flat surface and the circumference of the GB scaffolds are 78.53 mm^2 and 251 mm^2 respectively. The density measurement provided by the Helium (He) pycnometer equipment was 3.09 g/cc, therefore, the total volumetric porosity of the GB scaffold was identified as 57 vol%.

The volume of the GB scaffolds when accounting porosity is 135 mm^3. The increase of the pore volume of the LD samples is summarised in Table 2. Parallel and perpendicular drilling enhanced the pore volume of the GB samples by 10.1 %, and 22.5 % respectively, while the combined parallel and perpendicular drilling techniques increased the pore volume by 32.7 %. The overview of the physical properties of the reference and LD GB samples and the calculations are included in the Supplementary S3.1.

3.3. Surface profile of the GB scaffolds

The surface profile of the GB scaffolds was analysed using optical and confocal microscopies. The surface roughness analysis was carried out and these were found to be comparable in the range of 13.5 ± 0.3 μm, Fig. 8 A and B. Fig. 8 C and D demonstrate the longitudinal channels attributed to the natural porosity of the GB scaffolds and transverse LD holes respectively. The surface topography and natural porosity of the GB scaffolds are expected to provide the scaffolds with an increased surface area for cell adhesion and proliferation.

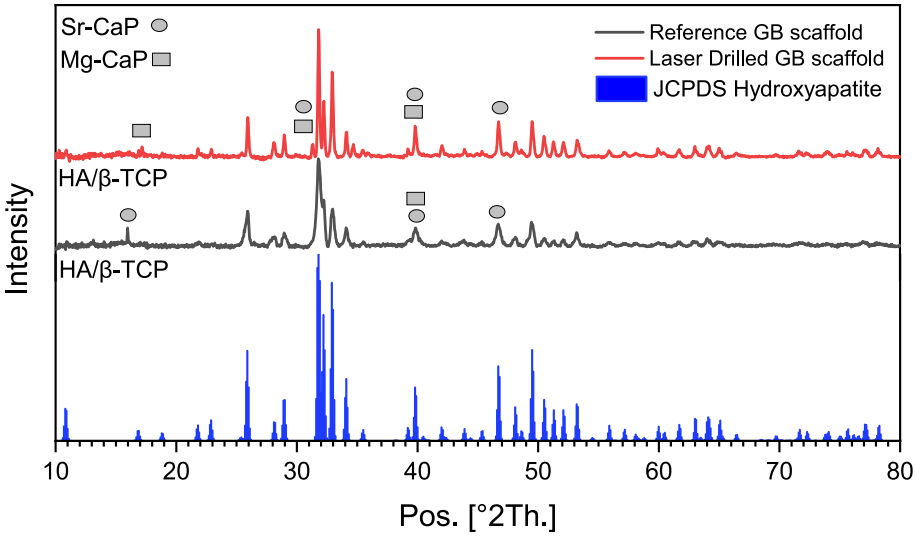

Fig. 5. XRD analysis on the Reference and LD GB scaffolds.

Table 2
A summary of the physical properties and pore increase for the LD GB scaffolds.

Parallel Drilling (D=10 mm, H=4mm)

No. Holes	Hole/ mm^2 of Sample	Area of Holes (mm^2)	Volume of Holes (mm^3)	Volume of sample accounting laser drilled channels (mm^3)	Pore Volume Increase (%)
0	0	0	0	0	–
4	19.5	1.52	6.08	128.9	4.5
5	15.6	1.90	7.60	127.4	5.6
6	13.0	2.28	9.12	125.9	6.7
9	8.7	3.42	13.68	121.3	10.1

Perpendicular Drilling (D=10 mm, H=4mm)

No. Holes	Hole/ mm^2 of Sample	Area of Holes (mm^2)	Volume of Holes (mm^3)	Volume of sample accounting laser drilled channels (mm^3)	Pore Volume Increase (%)
0	0	0	0	0	–
2	62.75	1.52	15.2	119.8	11.2
3	41.8	2.28	22.8	112.2	16.9
4	31.4	3.04	30.4	104.6	22.5

Parallel/ Perpendicular Drilling (D=10 mm, H=4mm)

No. Holes	Hole/ mm^2 of Sample	Area of Holes (mm^2)	Volume of Holes (mm^3)	Volume of sample accounting laser drilled channels (mm^3)	Pore Volume Increase (%)
9/4	–	–	44.08	90.9	32.7

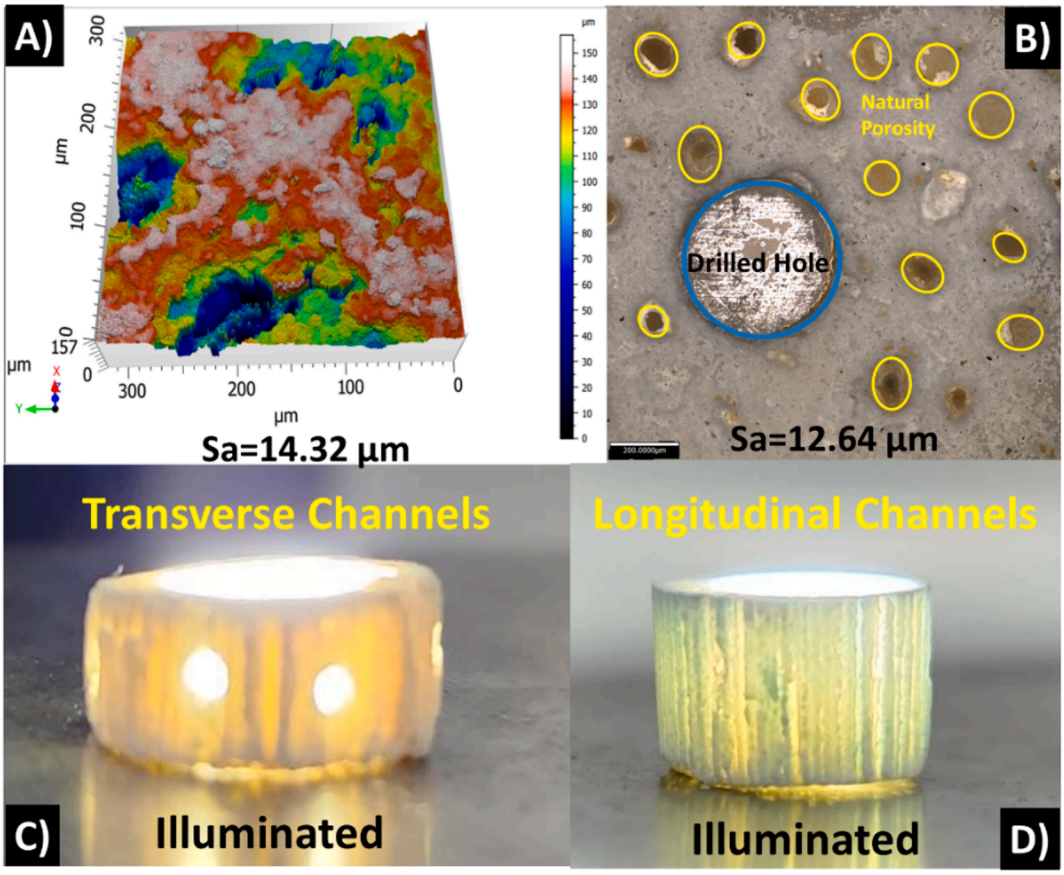

Fig. 6. The surface roughness of the GB scaffolds as measured by A) confocal microscopy and B) optical microscopy. C) The transverse laser drilled channels on the circumference of the GB scaffolds. D) The longitudinal channels characterising the structure of the GB scaffolds.

3.4. Scanning electron microscopy and energy dispersive X-ray spectroscopy

The microstructural and morphological analysis of the GB scaffolds was performed by scanning electron microscopy in secondary electron mode (Fig. 7-A). The unmodified scaffolds displayed anisotropic characteristics and advanced interconnected porosity, a structural arrangement which closely resembles the hierarchical organisation commonly found in the compact bone's osteonic system. The primary channels exhibited a complex tubular morphology with an average porous size of

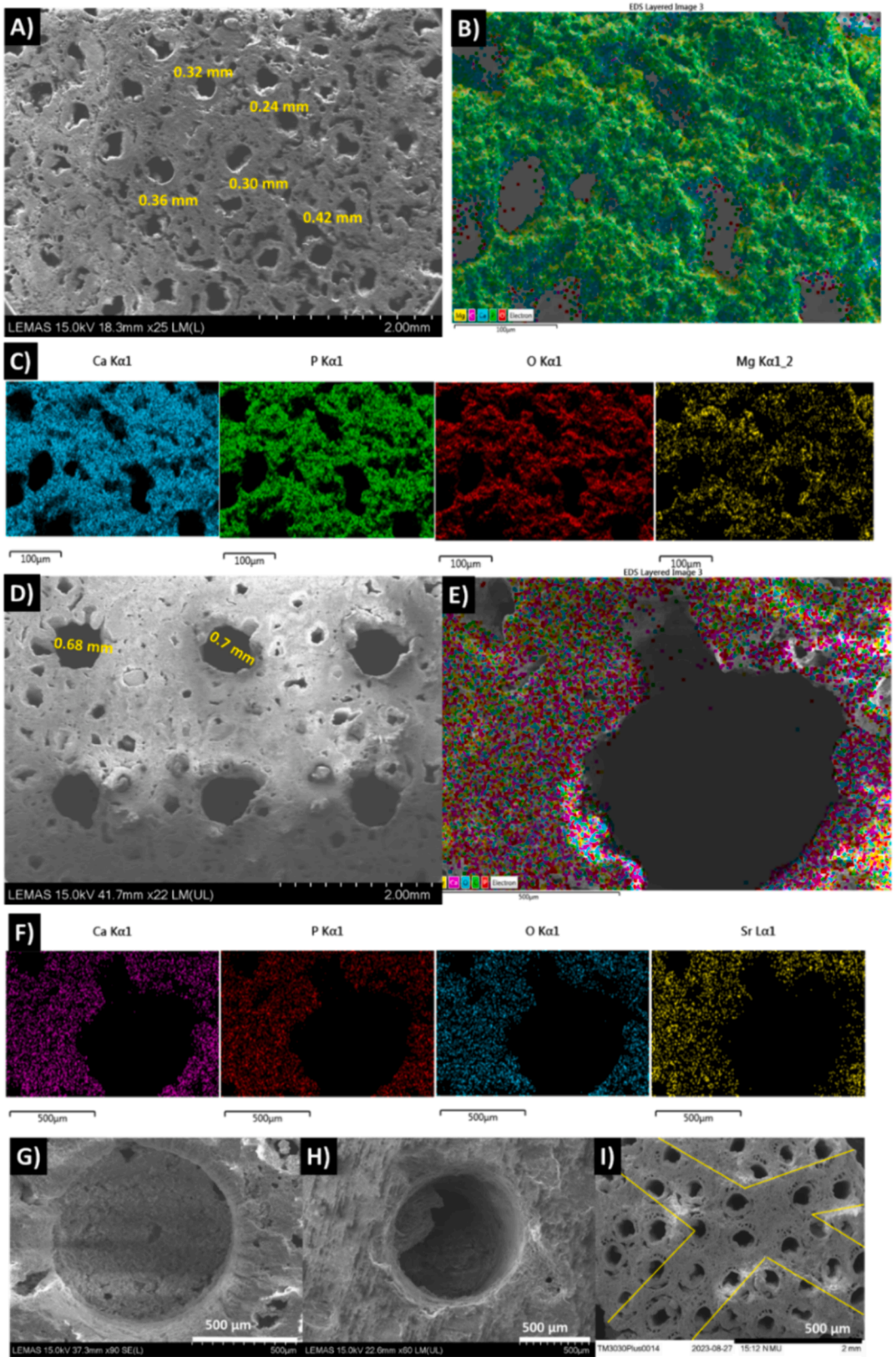

Fig. 7. A) The natural porosity of the GB scaffold has an average size of 0.33 μm. B) and C) EDS analysis on the unmodified scaffolds identified the phases of Calcium, Phosphorous, Oxygen, Carbon and Magnesium. D) The holes drilled by the water jet laser. E) and F) EDS analysis at the edges of the water jet laser drilled holes. G) A hole of 2 mm depth drilled by the femtosecond laser. H) Mechanically drilled hole. I) The cross-section of the drilled channels generated by water jet laser drilling.

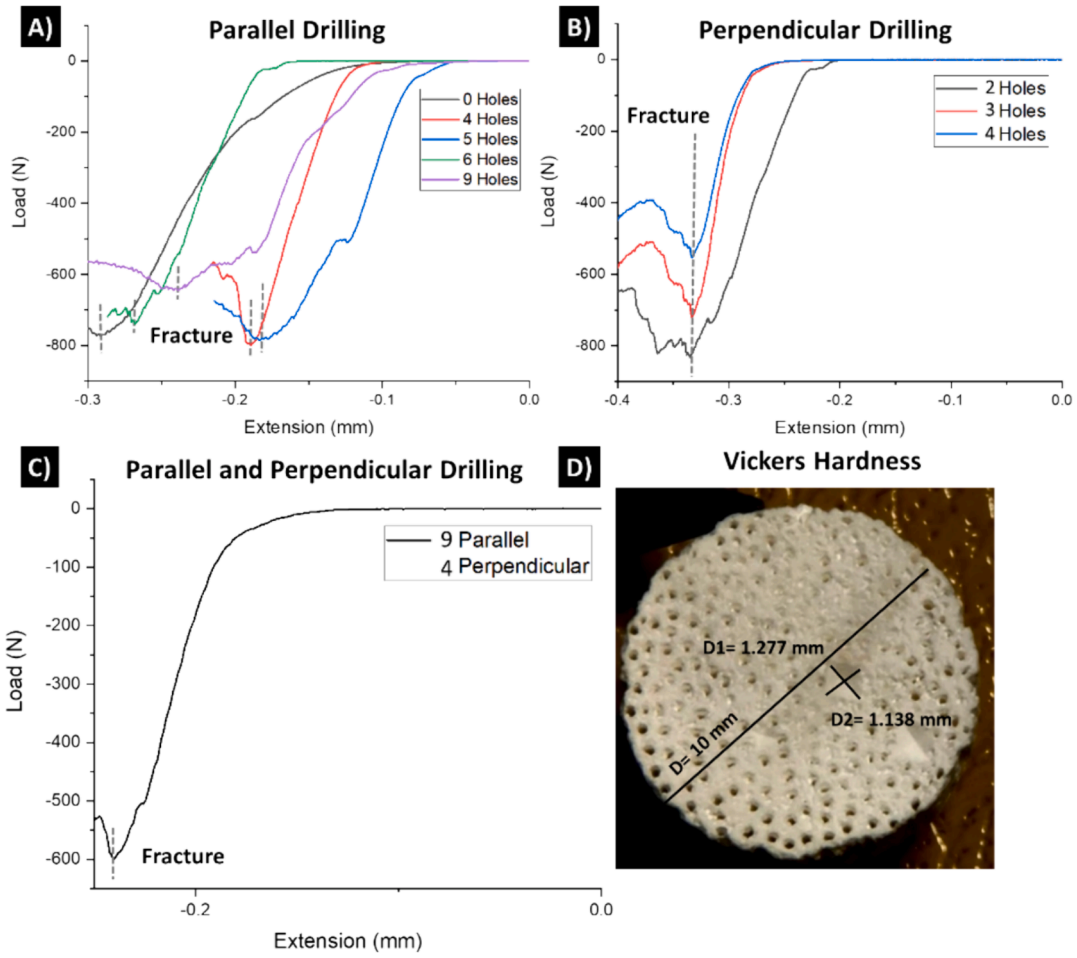

Fig. 8. A) The compressive strength of the unmodified and the parallel LD GB scaffolds containing 0, 4, 5, 6 and 9 holes. B) The compressive strength of perpendicularly LD GB scaffolds with 2, 3 and 4 holes. C) GB samples drilled with 9 parallel and 4 perpendicular holes. D) The Vickers micro-Hardness measurements of the GB scaffolds.

0.33 mm. The analysis carried out by the energy-dispersive X-ray spectroscopy identified phosphorous (P), calcium (Ca), and oxygen (O), corresponding to the $Ca_5(PO_4)_3OH$ and $Ca_3(PO_4)_2$ phases, detected by the XRD analysis. Magnesium (Mg) and Strontium (Sr) were also detected in the microstructure of the GB scaffolds, Fig. 7 – B, C.

The sub-mm drilled holes (0.7 mm) of Fig. 7-D generated by water jet laser drilling effectively enhanced the interconnected macro-porosity of the scaffolds, however slight shape distrortion and micro-cracks were observed at the edges of the drilled holes. EDS analysis performed at the edges of the drilled geometry also confirmed the lack of laser-drilling related contamination (Fig. 7-E, F). A hole drilled by the Ti sapphire femtosecond laser (D=10 mm, W=2 mm) is displayed in Fig. 7-G. The surface morphology of the hole drilled by the Ti sapphire laser presented a well-defined geometry, without the presence of cracks or distortion. A recast layer, potentially attributed to carbonisation, was observed at the circumference of the LD channel. The layer formation may be attributed to the effective number of pulses overlapping on the surface of the scaffolds at the scanning speed of 1 mm/s. When multiple pulses interact with the surface, the top surface will be ablated within a few initial pulses. The ablated particles from these initial pulses interact with the subsequent pulses, generating plasma; this process likely led to the formation of a recast layer on the circumferential zone. The recast layer formation could be reduced by adjusting the laser parameters.

Holes drilled by conventional drilling (D=0.7 cm, H=4 mm) did not present significant damage at the edges Fig. 7-H. The observation of the cross-section of the laser-drilled holes demonstrated that perpendicular drilling did not obstruct the natural porosity or the axial fibrous structure of the GB scaffolds, Fig. 7-I.

3.5. *Mechanical testing*

The average compressive strength of the unmodified scaffolds was approximately 10.18 MPa, Fig. 8-A. However, some unmodified GB samples exhibited compressive strength ranging between 8.91 MPa and 14.00 MPa Fig. 8-B, C, which was attributed to variations in the density distribution across the scaffolds. These variations resulted in the GB scaffolds absorbing different quantities of water, which along with the non-uniform distribution of the axial channels of the GB scaffolds generated varying compressive strength results.

The compressive strength of the parallelly drilled scaffolds containing 4 and 5 holes (10.18 ± 0.43 MPa) was identical to the unmodified scaffolds, Fig. 8-A. The 6-hole sample displayed a slightly reduced compressive strength of 9.05 ± 0.47 MPa, while the compressive strength of the 9-hole sample was reduced to 7.99 ± 0.62 MPa, Fig. 8-A. The reduction was attributed to drilling-induced micro-cracks and the narrower proximity of the holes in the 6 and 9 −hole samples.

The 2-hole perpendicularly drilled samples presented no compromise in their compressive strength 10.18 ± 0.43 MPa, Fig. 8-B. The 3-hole samples displayed a compressive strength of 9.20 ± 0.4 MPa, while the compressive strength of the 4-hole scaffolds was 7.34 ± 0.71 MPa. The GB scaffolds drilled with 9 parallel and 4 perpendicular holes demonstrated a compressive strength of 6.74 ± 1.25 MPa, Fig. 8-C. Perpendicular drilling had a more significant impact on compromising compressive strength of the GB scaffolds than parallel drilling. The

average compressive strength of each drilled sample is summarised in Table 3.

The Vickers micro-hardness of the reference GB scaffolds was measured as 37.4 HV (363 MPa) for a load of 3 kg, equation (2). Fig. 8-D illustrates the indentation spots positioned over areas of differing densities on the surface of the sample. The average length of the diagonals (D1 and D2, $D = \frac{D_1+D_2}{2} = 1.2075mm$) of the indentation spot was extrapolated from the length of the sample's diameter with the assistance of "Image J" software.

$$HV = 1.854\left(\frac{F}{D^2}\right) \quad (2)$$

3.6. In-vitro analysis of the drilled Green bone scaffolds

The *in vitro* analysis was carried out on the 4-hole perpendicularly LD GB scaffolds, on the basis that the samples provided the highest number of permissible transverse channels for complementing the axial porosity, without significantly compromising the compressive strength or structural integrity of the scaffolds, Fig. 9. The samples were produced through water jet laser drilling, since mechanical drilling contaminated the samples Supplementary S4.1. During contact cytotoxicity, Fig. 9 – 1, the laser-drilled scaffolds were evaluated for their ability to support cell growth, and proliferation. No signs of toxicity were observed after microscopic analysis, with no cytotoxic zone being seen as the cells proliferated up to and in contact with the scaffolds. The scaffolds have been graded as 0 with respect to ISO10993-5:2009, whereby the scaffolds displayed "no detectable zone around or under specimen". Fig. 9-2 demonstrates the results of LIVE/DEAD fluorescence staining of osteoblast G292 cells seeded onto laser-drilled scaffolds for 72 h. Cells proliferated over the entire surface of the scaffolds with >90 % cell viability. Cell attachment was visualised using Alexa Fluor-488 and DAPI fluorescent dyes, Fig. 9-3. All cells displayed consistent morphology across the surface of the GB scaffolds, with proliferation occurring evenly. G292 cells displayed normal cell morphology with no cell detachment or lysis. The laser-drilled GB scaffolds enabled a suitable environment for cell attachment and long-term cell proliferation. The results from the indirect extract cytotoxicity assay, Fig. 9-4, indicate cell viability greater than 95 % for the time points of 72 h, 1, 2, 3 and 4 weeks, signifying the LD GB scaffold's degradation products do not negatively affect cellular growth.

The migration of the G292 cells from the surface of the GB scaffolds to the inner walls of the LD channels was observed using LIVE/ DEAD fluorescent staining, Fig. 10 A, B and C. The 3D reconstructed confocal image exhibited G292 cells adhering to the walls of the laser drilled channel (0.7 mm), reaching a depth of 300 μm, 72 h after seeding. The depth to which cells migrated is greater than the average surface roughness of the GB scaffolds (13.5 μm, Fig. 6). The G292 cells also migrated inside the natural axial channels of the GB scaffolds Fig. 10 D, E and F.

Table 3
The compressive strength of the LD GB scaffolds produced by water jet laser drilling.

Samples/Holes	Average Compressive Strength (MPa)
0 Holes	10.21 ± 0.55
4 Parallel	10.38 ± 0.20
2 Perpendicular	10.32 ± 0.18
5 Parallel	10.33 ± 0.19
6 Parallel	9.19 ± 0.88
3 Perpendicular	9.26 ± 1.12
4 Perpendicular	7.39 ± 0.18
9 Parallel	8.05 ± 0.15
9 Parallel – 4 Perpendicular	6.74 ± 1.25

3.7. Degradation analysis

The degradation behaviour of the unmodified and LD GB scaffolds (average of N=3) at 2, 5 and 10 days is displayed in Fig. 11. The rate of mass loss was calculated according to equation (1) and is summarised in Table 4. Both types of GB scaffolds presented greater mass loss over the first 2 days (0.25 % Unmodified- 0.39 % LD), compared to day 5 (0.19 % Unmodified − 0.25 % LD) and day 10 (0.12 % Unmodified − 0.13 % LD). The LD GB scaffolds demonstrated a greater weight loss overall compared to the unmodified GB (0.58 % − 0.78 %).

The Raman spectra of the extracted solutions of the unmodified and LD GB scaffolds from days 2, 5 and 10, were compared to ones of pure GB and PBS, to identify whether minerals and ions were released in the PBS solution over the 3 time points. The Raman spectra of the GB scaffolds demonstrated symmetrical bending mode of (υ2) PO_4^{-3} ions at 429 and 448 cm^{-1} and antisymmetrical bending mode of (υ4) PO_4^{-3} ions at 578, 594, and 610 cm^{-1}. The extracted solutions from the LD GB scaffolds presented greater dissolution of minerals, as confirmed by the greater intensity peaks corresponding to the vibration of PO_4^{-3} ions, compared to the solutions from the unmodified scaffolds for all time points. The broad band of PBS~825 cm^{-1} was present in the Raman spectra of all solutions, which might be attributed to symmetric bending vibration of the (ν2-POH) A mode [29]. The 10-day solutions exhibited an additional band at 272 cm^{-1} which can be attributed to lattice vibrations of Ca-OH and Ca-PO_4.

4. Discussion

4.1. Composition of unmodified and Laser-Drilled Green bone samples

The compositional analysis of the GB scaffolds demonstrated that no contamination occurred post-laser drilling, as the diffractograms of both the unmodified and LD scaffolds were comparable, Fig. 5. Water jet laser drilling prevented: i) alterations in the composition of the GB scaffolds and ii) the introduction of drilling-related contamination. This is attributed to the high-pressure water jet: i) dissipating the heat generated during drilling, avoiding thermal damage and ii) removing debris and particulates during processing. All LD scaffolds exhibited the two major phases of $Ca_5(PO_4)_3OH$ and $Ca_3(PO_4)_2$, while the presence of Sr-CP and Mg-CP phases was attributed to a doping step in the manufacturing process of the scaffolds, described by Tampieri et al. [17].

During ultra-short laser pulse processing (fs laser drilling), the material's electron–phonon relaxation time is surpassed, leading to the formation of high-energy plasma. The volume of this plasma depends on the repetition rate of the laser, with colder plasma forming in high-repetition-rate lasers due to the lower energy per pulse. The transition from electron-phonon coupling to phonon–phonon coupling occurs in the 100 s pico to nanosecond regime, which facilitates thermal vibrations [20,30]. Microstructural analysis presented herein and elsewhere [7,27], confirmed minimal heat accumulation due to the lack of thermal damage to the LD scaffolds, also confirmed by EDS analysis. Laser processing induced evaporation at the focal point, forming craters, with linear polarization enhancing the ablation efficiency [23]. There was no to minimal contamination to the LD GB samples generated from water jet laser drilling and femtosecond laser drilling, in contrast to mechanical drilling which induced contamination to the drilled scaffolds, evident in the Supplementary S4.1.

Similarly to synthetic bone graft manufacturers across the literature, GB scaffolds mainly consist of hydroxyapatite ($Ca_{10}(PO_4)_6(OH)_2$) and $Ca_3(PO_4)_2$ β-tricalcium phosphate because it is bioactive and resembles natural bone apatite [14,16]. The composition, porosity and compressive strength of biomaterials in the literature are summarised in the Supplementary S1.1. The compositional constitution of the GB scaffolds is similar to that of commercial scaffolds by Bonesave™ (HA/β-TCP

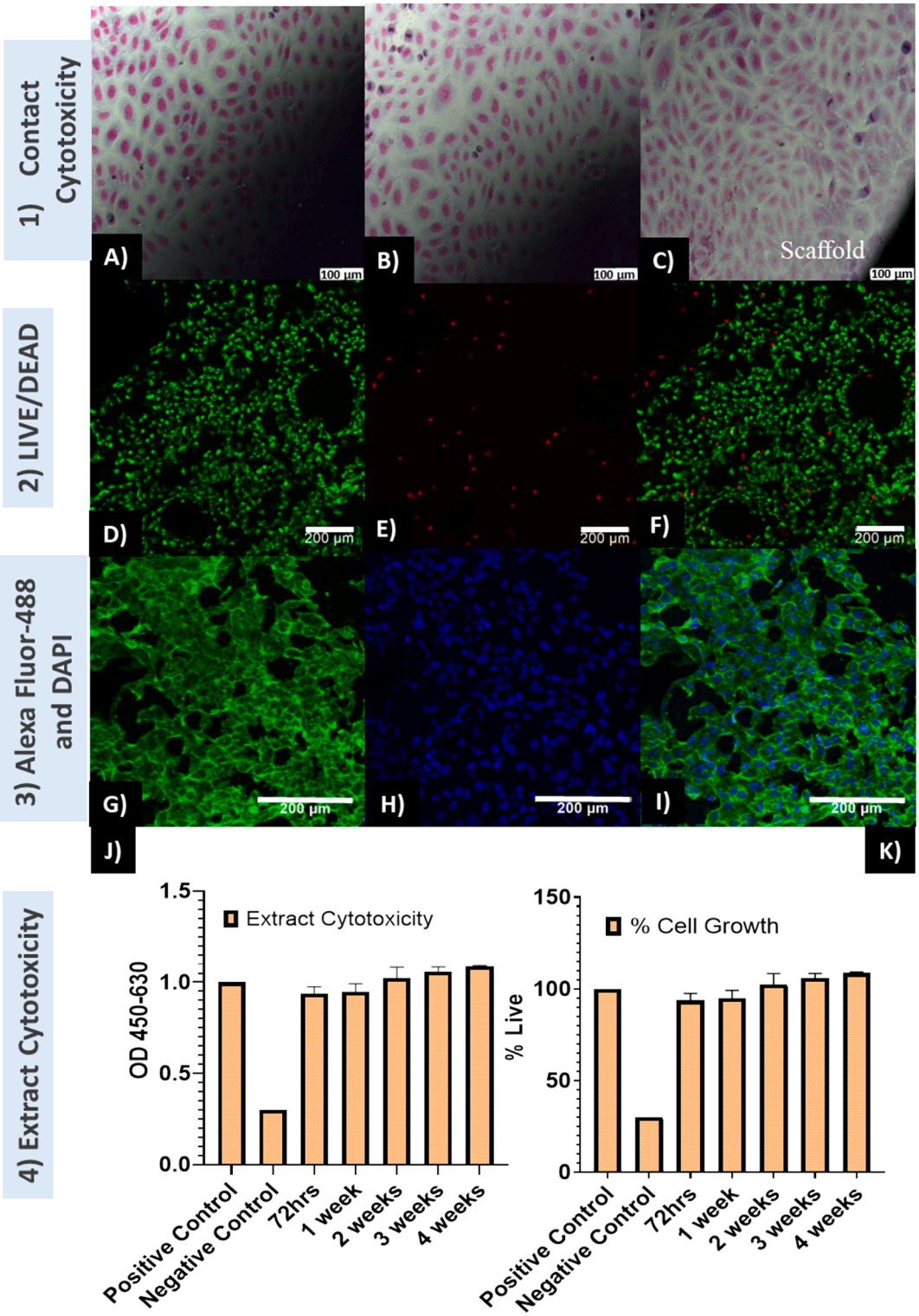

Fig. 9. 1) Green Bone scaffold contact cytotoxicity, per ISO10993-5:2009(E) of cultured osteoblast G292 cells (n = 3) for (A) 48 h, (B) 3 and (C) 7 days. The cells were stained with Giemsa solution and imaged on a Leica DM16000 B inverted microscope. 2) LIVE/DEAD staining of G292 osteoblast cells following 72 h on Green Bone Scaffolds; (D) depicts the live cells, (E) dead cells, and (F) depicts the combination of live and dead cells. 3) Presents the adhered cell line G292 osteoblast cells on the surface of the GB scaffolds, as observed by fluorescence microscopy. The cell seeding process lasted for 72 h, then the samples were fixed and were stained. Alexa Fluor-488 phalloidin indicated actin (green) and DAPI indicated the nucleic acids of the nuclei (blue). The cells were observed using an objective of (×20). 4) Demonstrates the results of extract cytotoxicity and proliferation performed on the Alpha MEM media mixed with 40 % DMSO, in which the seeded LD Green Bone scaffolds were placed. The extracts were collected after 1, 3 and 7 days, data represents mean + SD.

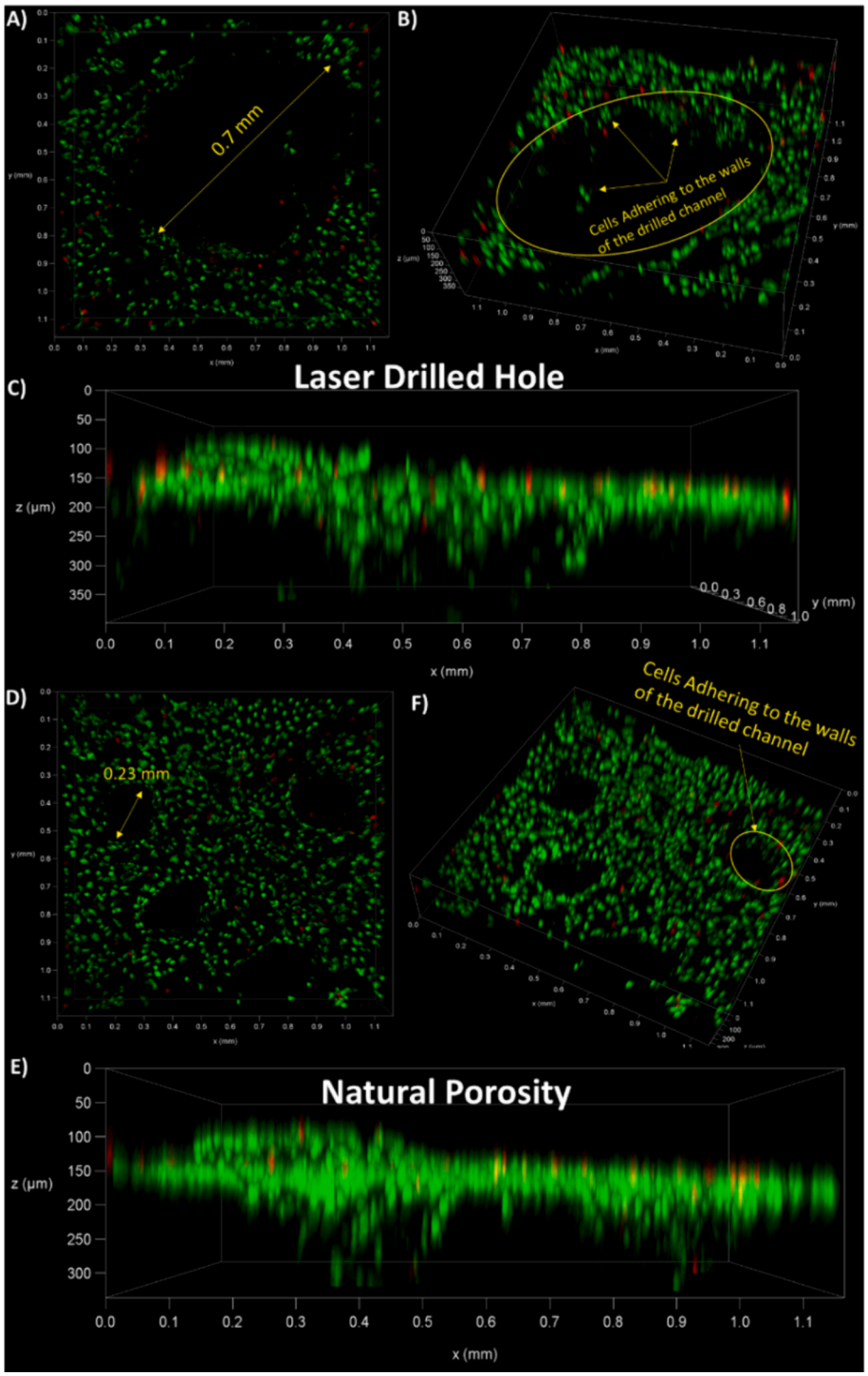

Fig. 10. 3D reconstructed image of the G292 cells stained with LIVE/ DEAD fluorescent dyes for observing cell migration on the walls of the laser-drilled channels, 72 h after seeding: A) Top view. B) Side View, C) Tilted top view. Cell migration in the axial channels of the Green Bone scaffolds D) Top view. E) Side View, F) Tilted top view.

(60:40)) and OsSatura™ BCP (HA/β-TCP) (80:20)) respectively [14], however they differ from the ones by ApaPore® and Endobon® that produce pure HA scaffolds.

4.2. Pore volume analysis of the GB scaffolds

The shape and distribution of the natural porosity of the GB scaffolds, which is characterised by large axial channels, allows fluid imbibition, including bone marrow aspirate, and permits the colonization of the entire scaffold [17,18]. Prior research on the application of the GB scaffolds in a clinical setting, raised concerns regarding the accelerated osteoconductivity of the graft via cell migration [2]. This was attributed to the migration of cells taking place primarily in the axial direction as a result of the intrinsic bio-morphogenic structure of the GB scaffolds, inherited from rattan wood [17,18]. In our research, we employed a nonintrusive laser processing approach to enhance the pore interconnectivity of the GB scaffolds, with the aim of facilitating and enhancing the flow of cells and fluids and the removal of waste products

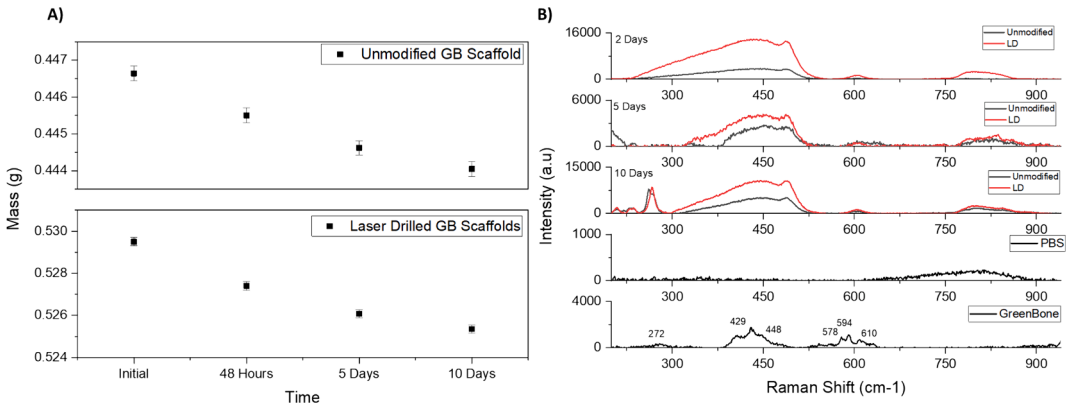

Fig. 11. A) Mass loss recorded for the unmodified and LD GB scaffolds placed in phosphate saline buffer solution with pH 7.4. The experiment was carried out at a physiological temperature of 37 °C. The average of 3 samples were tested per time point. B) Raman spectra of the GB scaffold, PBS and the day 2, 5 and 10 extracted solutions of the unmodified and LD GB scaffolds.

Table 4
The weight loss of the unmodified and LD GB scaffolds for the time points of 0, 2, 5 and 10 days.

Duration (Days)	Unmodified Scaffold Mass Loss (g)	LD ScaffoldMass Loss (g)
0–2	0.00255	0.00396
2–5	0.00197	0.00251
5–10	0.00128	0.00137
Total Weight Loss	0.00581	0.00784

throughout the graft, without compromising the structural integrity. The LD channels demonstrated a size ranging between 200 to 1000 μm, as sizes outside this spectrum could lead to suboptimal vascularisation or hinder the proximity needed for effective cell colony formation [18].

Among the laser drilling methods tested, waterjet laser drilling by the SYNOVA MCS 300 was considered the most effective method for machining the scaffolds in terms of accuracy and drilling speed. Waterjet laser drilling produced 700 μm diameter axial and transverse holes, that displayed slight micro-cracks at the edges. Fs laser drilling generated well-defined geometry holes of customised diameter, however, limitations regarding the focal length of the lens restricted the depth of the drilled holes to 2 mm. The material removal rate recorded during fs laser drilling was lower than the one of water jet laser drilling, due to the relatively low repetition rate used, 1 kH. The absence of significant heat transfer beyond the localized ablation area prevented the formation of cracks or thermal damage at the edges of the drilled holes. Mechanical drilling was also capable of producing 700 μm diameter through-holes, however localised damage was observed at the edges of the drilled geometries, evident from the SEM analysis. Mechanical drilling was not preferred over laser drilling as many scaffolds ended up breaking due to the vibrations generated by the drill bit while producing the through holes. This drilling method is expected to hinder the reproducibility and scaling up of the manufacturing process of drilled GB scaffolds.

Parallel and perpendicular drilling enhanced the pore volume of the scaffolds by 10.1 % (parallel drilling) and 22.5 % (perpendicular drilling) respectively. Meanwhile, the combination of parallel and perpendicular drilling enhanced the overall pore volume by 32.7 %.

All laser-drilled channels produced by the waterjet laser were suitable for accommodating cell proliferation. Microstructural analysis performed by SEM at secondary electron mode demonstrated that the natural porosity of the scaffolds was not disturbed by the laser process.

The relative porosity of the GB scaffolds in this research was comparable to α-BSM/Biobon® (50–60 %) and Bonesave™ (50–55 %) at 57 vol%. The enhanced pore interconnectivity of the GB scaffolds following laser drilling, is the highest among the literature (20–50 %) [14]. Such high interconnectivity is pivotal for bone regeneration, ensuring uniform cell distribution within the implant and promoting vascularisation.

4.3. Mechanical properties

The reference GB scaffolds exhibited an average compressive strength of 10.18 ± 0.43 MPa, albeit with some samples displaying variations ranging from 8.91 MPa to 14.00 MPa, possibly due to varying density regions across the GB scaffolds. The parallelly drilled scaffolds featuring 4 and 5 holes maintained a consistent compressive strength of approximately 10.18 ± 0.43 MPa. Beyond the 6-hole threshold, the compressive strength dropped to 9.05 ± 0.47 MPa, while the 9-hole sample displayed further reduction to 7.99 ± 0.62 MPa. For perpendicularly drilled scaffolds, the 2-hole samples retained their compressive strength of 10.18 ± 0.43 MPa. In contrast, the 3-hole samples exhibited a compressive strength of 9.20 ± 0.4 MPa, while the 4-hole scaffolds exhibited a decrease to 7.34 ± 0.71 MPa. The GB scaffolds containing both parallel and perpendicular drilled patterns presented a compressive strength of 7.34 ± 0.71 MPa. Perpendicular drilling had a more significant impact on reducing the compressive strength of the GB scaffolds compared to parallel drilling, however all drilled scaffolds retained their structural integrity after laser processing. The LD GB scaffolds did not demonstrate a decrease in their compressive strength for: i) hole per 15.6 mm^2 and ii) hole per 62.57 mm^2 in the cases of parallel and perpendicular drilling respectively, Table 2.

The unmodified and drilled GB scaffolds of the current research, displayed high compressive strength with respect to the literature Supplementary S1.1 [31]. Sprio et al. [18] confirmed that the unmodified biomorphic GB scaffolds exhibited a compressive strength of 9.8 MPa, aligning with the findings reported herein. The commercial scaffold from Kasios®, Atoll, consisting of sintered Hydroxyapatite + β-TCP (~25 %), demonstrated a compressive strength of 5.7 MPa as per Sprio et al [18]. Another 3D printed scaffold from calcium phosphate cement powder, by Gbureck et al. [32], presented 0.9 to 8.7 MPa compressive strength and can only claim higher compressive strength than the 3 and 4 perpendicular, 9 parallel and 9 parallel – 4 Perpendicular scaffolds. The compressive strength of the CPP bioceramic doped with potassium and strontium ions (K/Sr) by Xie et al. [33] was enhanced to 2.40 MPa, while the compressive strength of the BMSF/CPP and APSF/CPP scaffolds by Xie et al. [34], were 2.02 MPa and 2.41 MPa, respectively. The compressive strength of Landi et al.'s synthesised B-carbonate apatite (CHA) [35] was 6.0 MPa.

At last, the Vickers hardness of the GB scaffolds was identified as 37.4 HV, which is comparable with the Vickers hardness of the natural bone [36], 33.30 HV for the femoral head and 43.82 HV for the diaphysis.

4.4. In-vitro analysis

The osteoblast cells attached and proliferated on the scaffolds without eliciting toxicity, which could later be translated into the implant supporting physiological and anatomical functions within the body. *In vitro* analysis on the 4-hole perpendicularly laser-drilled GB scaffolds demonstrated excellent biocompatibility, with no observed cytotoxicity or adverse effects on cell growth, proliferation, or migration. According to ISO10993-5:2009 standards, the scaffolds received a rating of 0, indicating no detectable cytotoxic zone around or under the specimens. The indirect extract cytotoxicity assay consistently showed over 95 % cell viability at all tested time points. The rough surface of the GB scaffolds encouraged cell adhesion as observed via live/dead fluorescence staining, which revealed high cell viability (>90 %) and uniform cell proliferation across the scaffold surface. The 3D reconstructed LIVE/DEAD images confirmed cell proliferation and adhesion in the LD and axial pores of the GB scaffolds, at depth of ~300 μm, 72 h after seeding (Fig. 10).

4.5. GB scaffold degradation

The LD GB scaffolds presented greater mass loss compared to the unmodified scaffolds. At the 2-day point, the unmodified scaffolds presented a mass loss of 0.25 %, while LD scaffolds degraded by 0.39 %. On day 5, the weight loss was 0.19 % (unmodified) and 0.25 % (LD), and by day 10, the overall mass loss measured was 0.58 % (unmodified) and 0.78 % (LD). Raman analysis of the extracted solutions demonstrated that the LD GB scaffolds released more minerals and PO_4^{-3} ions in the PBS solution compared to the unmodified scaffolds potentially due to the increase in the surface area. The symmetrical and asymmetrical vibrations of the u2 and u4 PO_4^{-3} ions reported in this research match the findings of the literature [37,38]. The extracts from the 10-day time point presented a band at 272 cm^{-1} attributed to lattice vibrations of Ca-OH and Ca-PO_4. Biscaia et al. [39], reported a degradation rate of ~2–3 % per week for 3D-printed hydroxyapatite scaffolds sintered at 1300 °C. PLA/HA scaffolds degraded at about 1 % per week [40], while 3D-printed HA scaffolds exhibited a degradation rate of 2–3 % per week [41]. These rates are higher than those observed in our unmodified and LD GB scaffolds, possibly due to the lack of sintering during the manufacturing process and the static conditions under which the degradation experiments were carried out, which are not comparable to in-vivo conditions. This comparison highlights the relative stability of our scaffolds and the effectiveness of laser drilling in enhancing degradation rates, emphasising the effectiveness of the technology for applications requiring tailored scaffold resorption. Further degradation study is required to investigate the effect of laser drilling on the resorption of the GB material in order to optimise the resorption rate to match the regeneration rate of bone.

5. Conclusions

The study investigated the effect of laser drilling in enhancing the pore volume of the rattan wood-derived CE-marked GB scaffolds for improving the osteoconductivity, as the original morphogenic structure primarily allowed cellular and fluid transport in the axial direction.

- Water jet laser drilling was effective in improving the interconnecting porosity of the GB scaffolds, without: i) compromising the structural integrity and mechanical strength ii) inducing laser-related contamination, and iii) disrupting the longitudinal porosity of the GB scaffolds.
- Eight distinct sets of scaffolds with varied hole configurations were formed via water jet laser drilling. The volumetric porosity of the unmodified scaffolds was identified as 57 vol% while laser drilling increased the pore volume of the 4-hole perpendicularly drilled scaffolds, utilised for *in-vitro* analysis, by ΔV=22.5 %. The LD GB scaffolds presented greater mass loss compared to the unmodified GB scaffolds during resorption testing.
- The 4-hole perpendicularly drilled scaffolds demonstrated Vickers micro-hardness comparable to human bone (363 MPa) and compressive strength of 7.39 ± 0.18 MPa.
- The laser-drilled GB scaffolds were not toxic to osteoblast G292 cells. The LD scaffold extracts did not possess any negative impediment to cellular (>95 %) cell viability. LIVE/DEAD cell fluorescence analysis also verified cell viability (>90 %). Osteoblast G292 cells presented even proliferation over the rough surface and in the pores of the scaffolds. The 3D LIVE/ DEAD reconstructed images presented evidence of cell migration in the LD channels and the natural pores.

Funding

This research was jointly funded by the GreenBone Ortho Company, by The Engineering and Physical Sciences Research Council (EPSRC), Project Reference No. 1787225, The Medical Research Council: MRC-CIC-L42017/ PO4050781788 and the Biomedical Research Centre (NIHR-20331).

CRediT authorship contribution statement

Evangelos Daskalakis: Writing – review & editing, Writing – original draft, Visualization, Validation, Methodology, Investigation, Formal analysis, Data curation. **Neelam Iqbal:** Writing – review & editing, Validation, Formal analysis, Data curation. **Sarathkumar Loganathan:** Writing – review & editing, Formal analysis, Data curation. **Emilio Spettoli:** Writing – review & editing, Resources. **Giacomo Morozzi:** Writing – review & editing, Resources. **Alberto Ballardini:** Writing – review & editing, Resources. **Peter V. Giannoudis:** Writing – review & editing, Supervision, Project administration, Investigation, Funding acquisition, Conceptualization. **Animesh Jha:** Writing – review & editing, Supervision, Project administration, Funding acquisition, Conceptualization.

Declaration of competing interest

The authors declare that they have no known competing financial interests or personal relationships that could have appeared to influence the work reported in this paper.

Data availability

Data will be made available on request.

Acknowledgements

The authors acknowledge GreenBone Ortho, Faenza, Italy for providing the samples required for testing and characterisation. The authors also acknowledge the University of Leeds for providing the facilities and equipment for drilling and characterising the samples, along with the technicians Robbert Simpson, Tony Wiese and Graham Brown.

Appendix A. Supplementary data

Supplementary data to this article can be found online at https://doi.org/10.1016/j.matdes.2024.113243.

References

[1] R.J. Cuthbert, et al., Regulation of angiogenesis discriminates tissue resident MSCs from effective and defective osteogenic environments, J Clin Med 9 (6) (2020).
[2] . Ganguly, P., et al., Evaluation of human bone marrow mesenchymal stromal cell (MSC) functions on a biomorphic rattan-wood-derived scaffold: a comparison between cultured and uncultured MSCs. 2022. **9**(1): p. 1.

[3] P. Lafforgue, Pathophysiology and natural history of avascular necrosis of bone, Joint Bone Spine 73 (5) (2006) 500–507.
[4] Kouroupis, D., et al., Native multipotential stromal cell colonization and graft expander potential of a bovine natural bone scaffold. 2013. **31**(12): p. 1950-1958.
[5] Takahashi, N., et al., *Osteoblastic cells are involved in osteoclast formation.* 1988. **123** (5): p. 2600-2602.
[6] Suda, T., N. Takahashi, and T.J.J.E.r. Martin, *Modulation of osteoclast differentiation.* 1992. **13**(1): p. 66-80.
[7] Anastasiou, A., et al., *Exogenous mineralization of hard tissues using photo-absorptive minerals and femto-second lasers; the case of dental enamel.* 2018. **71**: p. 86-95.
[8] Fillingham, Y., J.J.T.b. Jacobs, and j. journal, *Bone grafts and their substitutes.* 2016. **98**(1_Supple_A): p. 6-9.
[9] H. Dinopoulos, R. Dimitriou, P.V. Giannoudis, Bone graft substitutes: What are the options? Surgeon 10 (4) (2012) 230–239.
[10] Miron, R.J., et al., *Osteoinductive potential of a novel biphasic calcium phosphate bone graft in comparison with autographs, xenografts, and DFDBA.* 2016. **27**(6): p. 668-675.
[11] C.M. Murphy, M.G. Haugh, F.J. O'Brien, The effect of mean pore size on cell attachment, proliferation and migration in collagen–glycosaminoglycan scaffolds for bone tissue engineering, Biomaterials 31 (3) (2010) 461–466.
[12] S.J. Hollister, Porous scaffold design for tissue engineering, Nat. Mater. 4 (7) (2005) 518–524.
[13] F. Zhao, T. Ma, Perfusion bioreactor system for human mesenchymal stem cell tissue engineering: Dynamic cell seeding and construct development, Biotechnol. Bioeng. 91 (4) (2005) 482–493.
[14] Hing, K.A., Bioceramic bone graft substitutes: influence of porosity and chemistry. 2005. **2**(3): p. 184-199.
[15] Al-allaq, A.A. and J.S. Kashan, A review: In vivo studies of bioceramics as bone substitute materials. 2023. **4**(2): p. 123-144.
[16] L. Schröter, et al., Biological and mechanical performance and degradation characteristics of calcium phosphate cements in large animals and humans, Acta Biomater. 117 (2020) 1–20.
[17] Tampieri, A., et al., *Heterogeneous chemistry in the 3-D state: an original approach to generate bioactive, mechanically-competent bone scaffolds.* 2019. **7**(1): p. 307-321.
[18] S. Sprio, et al., Hierarchical porosity inherited by natural sources affects the mechanical and biological behaviour of bone scaffolds, J. Eur. Ceram. Soc. 40 (4) (2020) 1717–1727.
[19] S. Paderni, S. Terzi, L. Amendola, Major bone defect treatment with an osteoconductive bone substitute, Musculoskel. Surg. 93 (2) (2009) 89–96.
[20] Führa, B., et al. *High precision drilling with ultra-short laser pulses*. in *Proceedings of the Lasers in Manufacturing Conference*. 2017.
[21] Rahmani-Monfard, K., A. Fathi, and S.M.J.T.I.J.o.A.M.T. Rabiee, *Three-dimensional laser drilling of polymethyl methacrylate (PMMA) scaffold used for bone regeneration.* 2016. **84**: p. 2649-2657.
[22] Song, Y., et al., *Real-time spectral response guided smart femtosecond laser bone drilling.* 2020. **128**: p. 106017.
[23] S. Loganathan, et al., Surface processing: an elegant way to enhance the femtosecond laser ablation rate and ablation efficiency on human teeth, Lasers Surg. Med. 51 (9) (2019) 797–807.
[24] S. Loganathan, et al., Prediction of femtosecond laser ablation profile on human teeth, Lasers Med. Sci. 34 (4) (2019) 693–701.
[25] C. Fornaroli, J. Holtkamp, A. Gillner, Laser-beam helical drilling of high quality micro holes. in International Congress on Applications of Lasers & Electro-Optics, AIP Publishing, 2012.
[26] H. Uchtmann, C. He, A. Gillner, High precision and high aspect ratio laser drilling: challenges and solutions. High-Power Laser Materials Processing: Lasers, Beam Delivery, Diagnostics, and Applications V, SPIE, 2016.
[27] A.D. Anastasiou, et al., Sintering of calcium phosphates with a femtosecond pulsed laser for hard tissue engineering, Materials & Design 101 (2016) 346–354.
[28] E. Daskalakis, A. Scott, A. Jha, Enhancing the ignitability of the Al–TiO2–B2O3 powder mixture through intensive vibratory ball milling (C:P12), Ceramics Internat. 49 (14, Part B) (2023) 24142–24155.
[29] K.A. Syed, et al., Micro-Raman observation on the HPO42– association structures in an individual dipotassium hydrogen phosphate (K2HPO4) droplet, J. Phys. Chem. A 116 (6) (2012) 1558–1564.
[30] G.D. Gautam, A.K. Pandey, Pulsed Nd:YAG laser beam drilling: A review, Optics Laser Technol. 100 (2018) 183–215.
[31] M. Vlasea, R. Pilliar, E. Toyserkani, Control of structural and mechanical properties in bioceramic bone substitutes via additive manufacturing layer stacking orientation, Add. Manuf. 6 (2015) 30–38.
[32] Gbureck, U., et al., *Resorbable Dicalcium Phosphate Bone Substitutes Prepared by 3D Powder Printing.* 2007. **17**(18): p. 3940-3945.
[33] H. Xie, et al., Application of K/Sr co-doped calcium polyphosphate bioceramic as scaffolds for bone substitutes, J. Mater. Sci. Mater. Med. 23 (4) (2012) 1033–1044.
[34] H. Xie, et al., A novel bioceramic scaffold integrating silk fibroin in calcium polyphosphate for bone tissue-engineering, Ceram. Internat. 42 (2, Part A) (2016) 2386–2392.
[35] E. Landi, et al., Carbonated hydroxyapatite as bone substitute, J. Eur. Ceram. Soc. 23 (15) (2003) 2931–2937.
[36] W.W. Wu, et al., Bone hardness of different anatomical regions of human radius and its impact on the pullout strength of screws, Orthop Surg 11 (2) (2019) 270–276.
[37] U. Anjaneyulu, D.K. Pattanayak, U. Vijayalakshmi, Snail shell derived natural hydroxyapatite: effects on NIH-3T3 cells for orthopedic applications, Mater. Manuf. Proc. 31 (2) (2016) 206–216.
[38] M. Raii, Formulation, caracterization and implementation of permeable reactive barriers based on calcium phosphate Formulation, caractérisation et mise en œuvre des barrières perméables réactives à base de phosphate de calcium, utilisation pour la fixation de polluants, Institut National Polytechnique de Toulouse - INPT, 2012.
[39] S. Biscaia, et al., 3D Printed Poly, Internat. J. Mol. Sci. 23 (4) (2022) 2318.
[40] S. Zohoor, N. Abolfathi, M. Solati-Hashjin, Accelerated degradation mechanism and mechanical behavior of 3D-printed PLA scaffolds for bone regeneration, Iran. Polymer J. 32 (10) (2023) 1209–1227.
[41] A. Thurzo, et al., Fabrication and in vitro characterization of novel hydroxyapatite scaffolds 3D printed using polyvinyl alcohol as a thermoplastic binder, Internat. J. Mol. Sci. 23 (23) (2022) 14870.